Manufacturing Letters 23 (2020) 1–4

Contents lists available at ScienceDirect

Manufacturing Letters

journal homepage: www.elsevier.com/locate/mfglet

External-energy-assisted nanomachining with low-stiffness atomic force microscopy probes

Huimin Zhou [a], Christopher Dmuchowski [b,c], Changhong Ke [b,c], Jia Deng [a,*]

[a] Department of Systems Science and Industrial Engineering, Binghamton University, Binghamton, NY 13902 United States
[b] Department of Mechanical Engineering, Binghamton University, Binghamton, NY 13902 United States
[c] Materials Science and Engineering Program, Binghamton University, Binghamton, NY 13902 United States

ARTICLE INFO

Article history:
Received 7 August 2019
Received in revised form 11 October 2019
Accepted 15 November 2019
Available online 16 November 2019

Keywords:
AFM-based nanomachining
Nanomanufacturing
Low-stiffness probe
Ultrasonic vibration
Joule heating
Adhesion force

ABSTRACT

Thermal atomic force microscope (AFM) nanolithography enables many nanofabrication applications, but it requires special thermal probes. In this paper, we developed a vibration-assisted sample heating approach to implement the nanomachining of poly(methyl methacrylate) (PMMA) with a regular AFM probe with low stiffness (~0.16 N/m). The joule heating softens the PMMA, which lowers the normal force. The in-plane vibration with high frequency was applied to reduce the adhesion force between the AFM tip and the PMMA with elevated temperature, which enhances nanomachining performances. By using this approach, uniform nanopatterns with controllable dimensions were fabricated on PMMA films with small setpoint force.

Published by Elsevier Ltd on behalf of Society of Manufacturing Engineers (SME).

1. Introduction

Driven by many applications, atomic force microscope (AFM)-based nanomanufacturing has been applied to perform nanometer-scale surface modification using the fabrication capability of the sharp tip on the probe [1,2]. As an alternative low-cost and low-effort technique for high-resolution optical and electron-beam lithography, it enables fabrications of nanostructures in the sub-50 nm regime [3], which include metals (aluminum and copper) [4], metalloid (silicon) [5], and polymers (Poly(methyl methacrylate)(PMMA)) [6–10].

One of the nanopatterning methods is vibration-assisted nanomachining [11,12]. In-plane and out-of-plane vibrations of the samples enable tunable nanomachining processes [3,8,13] and complex geometries [7,14] with reduced tip wear [15]. Vibration-assisted nanomachining is able to increase the patterning speed and to enhance the nanomachining performance. But, to our best knowledge, it has not been integrated with thermal energy, which has the potential to further reduce the force and tip wear when fabricating the same patterns.

Another method is the thermo-mechanical writing [16,17]. Generally, thermal fields can facilitate the patterning of soft materials such as polymers, reduce tip wear during mechanical deformation, and therefore assist thermo-mechanical processes [18]. However, the adhesion force between various types of AFM tips and samples can be significantly higher as temperature increases [19–21], which degrade the manufacturing performance. Stiff AFM probes can avoid the adhesion for thermal mechanical nanomanufacturing but they usually generate uncontrollably deeper and irregular trenches [21]. It is not easy to apply small but accurate normal forces on samples because of their large spring constants. Thermal fields applied in AFM can be either cantilever heating [22–24] or sample heating [25]. Compared with cantilever heating, sample heating method has the potential to improve the lithography speed and efficiency by eliminating the thermal transfer process between the tip and the sample when the entire sample surface is heated.

In this paper, we present an external-energy-assisted (mechanical vibration and sample heating) nanomachining method using soft AFM cantilevers. The integration of heating and vibration energy were utilized to enhance the nanomachining performances. The trench profiles became controllable and uniform without negative impacts of surface adhesion under elevated temperatures using low-stiffness probes. Meanwhile, this method enables the control of the fabricated pattern dimensions on demand, which is critical for the fabrication of complex patterns with high efficiency.

* Corresponding author.
E-mail address: jiadeng@binghamton.edu (J. Deng).

https://doi.org/10.1016/j.mfglet.2019.11.001
2213-8463/Published by Elsevier Ltd on behalf of Society of Manufacturing Engineers (SME).

2. Experimental setup

The experimental setup is based on a commercial AFM system (NTEGRA, NT-MDT) with sample heating function, as shown in Fig. 1. Two one-directional shear piezo actuators (PL5FBP3, Thorlabs) were attached on the heating stage (for generating vibrations in both × and y directions). The nanomachining tests were conducted on a 100-nm thick PMMA (950PMMA A4) film, which was spin coated on a cleaned silicon substrate for 60 s at 4000 rpm, and was then post baked at 180 °C for 90 s. The sample was fixed on the top of actuators and heated up to 45 °C by using the sample holder. We used double-sided adhesive sheets (Therm O Web) for the attachment between sample holder, piezo stack, and the sample. The input sinusoidal signal was transferred from a function generator to actuate the xy piezos. An amplifier with a gain of 20 was incorporated in the system to obtain larger vibration amplitude and thus larger trench width.

The employed AFM probes (CSG10 from NT-MDT) possess a nominal tip radius of ~10 nm and a nominal spring constant of 0.16 N/m. Each employed AFM probe was calibrated using a thermal-tuning method. Constant forces were applied on the sample surface during the lithography process in contact mode.

The AFM tip-sample adhesion force F, is calculated based on the measured force-distance curves [26] and is given as

$$F = (SP - DFL)/SR * K \quad (1)$$

where SP is the setpoint (nA), DFL is the cantilever deflection (nA), SR is the sensor response (nA/nm), which refers to the gradient between Points A and B in Fig. 2(a), and K is the measured spring constant (N/m).

3. Experimental results and discussions

A comparison of the adhesion forces between an AFM tip and a sample surface was performed with and without vibration (2 MHz) under different temperatures of the sample holder (30, 35, 40, and 45 °C). The temperatures of the sample holder are closed loop controlled. But there are thermal losses after transferring onto the sample surfaces. We measured the temperatures of sample surface using a thermocouple after being stable: 30, 35, 40, and 45 °C of the sample holder corresponds to 28, 30, 32.5, and 37 °C of the sample surface. As previously mentioned, the adhesion force is calculated from the straight-line fit of the force-distance curve. The tip wear during the measurement of the force-distance curves is ignored, and the sensor response and the force constant are assumed to be the same between different measurements. The comparison of the adhesion force can be transformed into the comparison of the distance between Points B and C in Fig. 2(a).

Fig. 2(b) shows the results of the adhesion force comparison experiments from 35 to 40 °C. With no vibration, the adhesion force between the tip and the sample surface keeps increasing as the temperature increases. In the meantime, the adhesion force becomes smaller as the vibration is applied, and the decrease of adhesion force between experiments with and without vibration increased from 49%, 52%, 53%, to 59% under 30, 35, 40, and 45 °C, respectively. Therefore, the effect of vibration on reducing tip adhesion becomes more significant under high temperature.

To further investigate the effect of different parameters on the nanopattern geometry, we designed a factorial experiment with vibration amplitude and loading force as two factors, each with two levels. The high level and low level of loading force are 20 nA and 10 nA (about 339 nN and 169 nN, respectively). The two levels of vibration input amplitude are 3.5 V and 7 V, which correspond to the actual output amplitude of 70 V and 140 V, respectively, on the piezo. The vibration frequency is 2 kHz, and the direction of vibration is vertical to the machining direction. All the experiments were performed under 40 °C, with a tip moving speed of 0.5 μm/s. Fig. 3 shows the AFM image of the nanomachined patterns with different levels of amplitude and loading force.

According to the analysis of variance (ANOVA) results based on data in Table 1, both the vibration amplitude and setpoint have significant impacts on trench width (with p-values of 0.000 and 0.001, respectively). The p-value of the interaction between two factors is found to be 0.269, which shows that the interaction does not have statistical significance. Trench width increases along with the increase of setpoint and amplitude, which improves the machining efficiency. Uniform trenches with controllable depth and width also indicates an improvement in machining performances. According to the calculated regression equation, the trench width and depth can be predicted by the applied vibration amplitude and setpoint, which are given as follows:

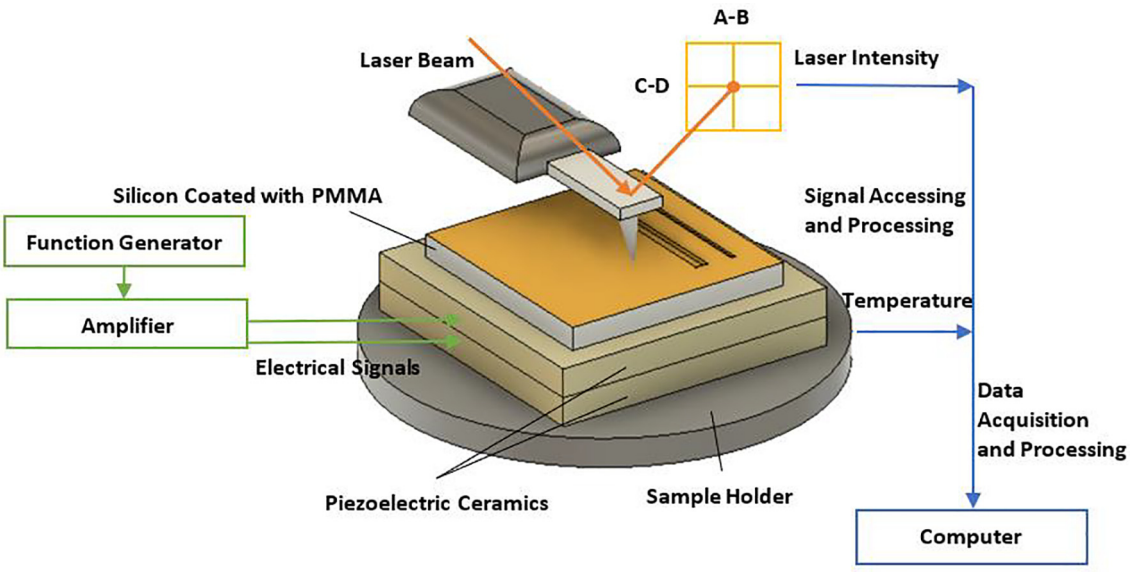

Fig. 1. Diagram of experimental setup.

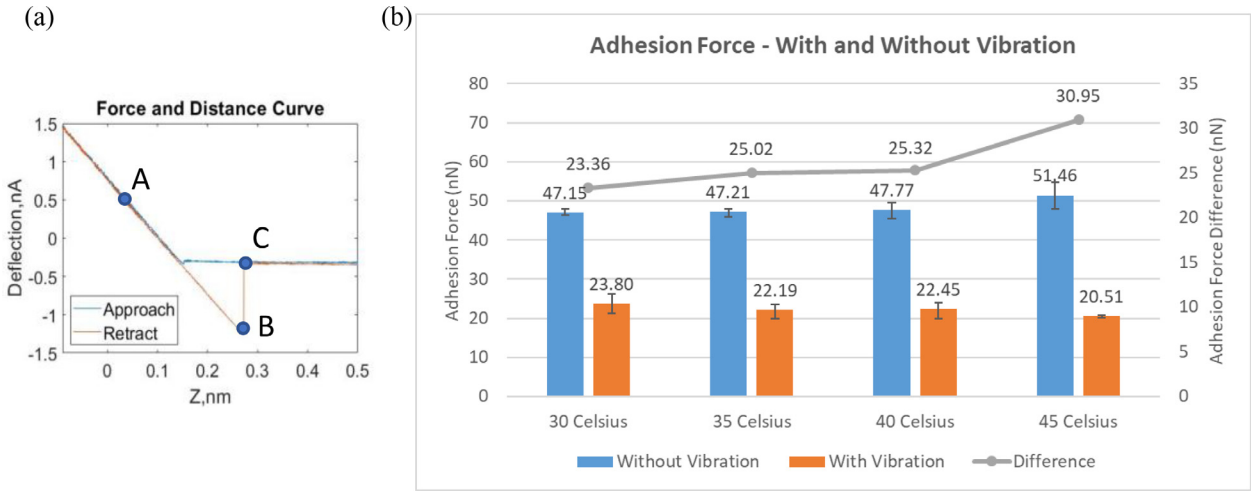

Fig. 2. (a) A typical force-distance curve that is used to calculate the surface adhesion force. (b) Comparison of the adhesion force with and without vibration under different temperatures (vibrational frequency and amplitude are 2 MHz and 80 V, respectively).

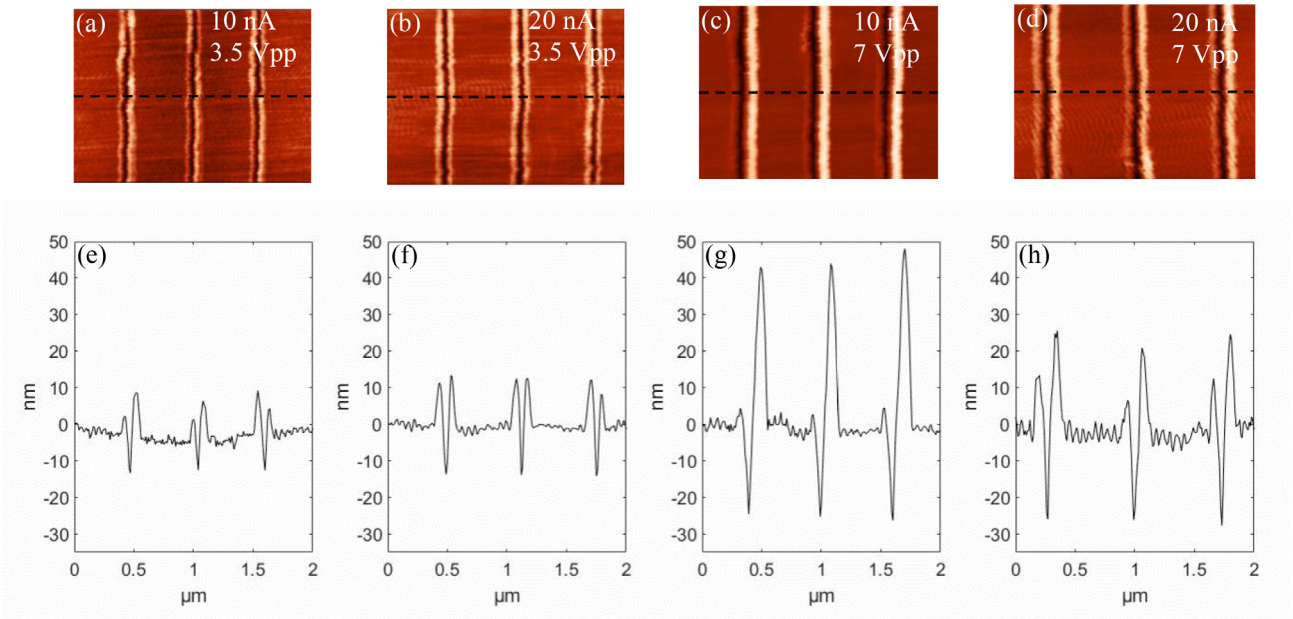

Fig. 3. (a)–(d) AFM images of nanomachining patterns on PMMA film: (a) Amplitude = 3.5 V, setpoint = 10 nA; (b) Amplitude = 3.5 V, setpoint = 20 nA; (c) Amplitude = 7 V, setpoint = 10 nA; (d) Amplitude = 7 V, setpoint = 20 nA. (e)–(h) Cross-sectional profiles of trenches in (a)–(d) under different amplitudes and loading forces, respectively.

$$\begin{aligned} \textit{Width}\ (\text{nm}) = &-5.2 + 9.46 * \textit{Amplitude}\ (\text{V}) + 0.05 * \textit{Setpoint}\ (\text{nA}) \\ &+ 0.1057 * \textit{Amplitude}\ (\text{V}) * \textit{Setpoint}\ (\text{nA}), \end{aligned}$$

$$\begin{aligned} \textit{Depth}\ (\text{nm}) = &-16.77 + 5.24 * \textit{Amplitude}\ (\text{V}) + 0.634 \\ &* \textit{Setpoint}\ (\text{nA}) + 0.0267 * \textit{Amplitude}\ (\text{V}) \\ &* \textit{Setpoint}\ (\text{nA}). \end{aligned}$$

The results show that the feature depths increase along with the widths. The tip has an inverted pyramid shape, larger vibration amplitude may horizontally push the edges of the soft tip and thus generate a normal force that can vibrate the tip up and down, leading to the depth increase.

4. Conclusions

In this study, we investigated the external-energy-assisted nanomachining of PMMA that uses AFM probes with very low spring constants. We introduced the joule heating to facilitate the nanomachining process due to the softening of polymers as temperature increases. In-plane vibration was applied to the sample to increase the machining efficiency and to decrease the surface adhesion that increases along with the temperature. We also investigated the effect of vibration amplitude and loading force on the trench width and depth. Trenches will become wider and deeper as the increase of vibration amplitude, which may because of the torsion of the AFM cantilever during nanomachining. The contributions of this study are twofold. First, we enable the nanomachining with a soft contact cantilever on polymer surfaces under elevated temperatures, while very few studies used AFM tips with similar stiffness in nanomachining and obtained more than 10 nm depth of trench on the polymer surface. Second, we applied vibration on the xy plane to reduce the surface adhesion generated by thermal effect, to increase machining efficiency, and to improve the overall performance that includes better finish and uniform trenches.

Table 1
Experimental trench widths and depths under different amplitudes and setpoints.

Amplitude (V)	Setpoint (nA)	Width (nm)	Depth (nm)	Amplitude (V)	Setpoint (nA)	Width (nm)	Depth (nm)
3.5	10	30.0	8.1	7	10	75.0	30.1
3.5	10	30.0	8.1	7	10	60.0	30.2
3.5	10	34.0	9.7	7	10	74.0	23.4
3.5	10	40.0	9.4	7	10	70.0	25.9
3.5	10	32.0	7.6	7	10	70.0	31.3
3.5	10	35.0	7.7	7	10	79.0	31.2
3.5	10	35.0	10.0	7	10	71.0	24.8
3.5	10	30.0	9.9	7	10	65.0	23.9
3.5	10	29.0	8.5	7	10	55.0	28.5
3.5	10	26.0	9.7	7	10	70.0	31.9
3.5	20	45.0	12.3	7	20	72.0	30.3
3.5	20	40.0	21.5	7	20	80.0	36.5
3.5	20	40.0	16.0	7	20	81.0	35.0
3.5	20	30.0	16.2	7	20	80.0	33.7
3.5	20	38.0	19.3	7	20	69.0	32.0
3.5	20	34.0	18.3	7	20	71.0	26.7
3.5	20	36.0	18.2	7	20	80.0	42.2
3.5	20	35.0	13.5	7	20	80.0	44.8
3.5	20	35.0	12.3	7	20	77.0	32.3
3.5	20	30.0	13.7	7	20	78.0	49.8

Declaration of Competing Interest

The authors declare that they have no known competing financial interests or personal relationships that could have appeared to influence the work reported in this paper

Acknowledgements

This work was supported in part by the startup funds from Binghamton University, and by the Small Scale Systems Integration and Packaging (S3IP) Centre of Excellence, funded by New York Empire State Development's Division of Science, Technology and Innovation. The AFM measurements were performed using a facility that was acquired through an NSF-MRI Award (CMMI-1429176). C.M.D acknowledges fellowship support from the New York NASA Space Grant Consortium.

References

[1] Staufer U, Kern DP. A scanning tunneling microscope based microcolumn system. Jpn J Appl Phys 1992;31(12 S):4232–4240.
[2] Hu H, Kim HJ, Somnath S. Tip-based nanofabrication for scalable manufacturing. Micromachines 2017;8(3).
[3] Zhang L, Dong J. High-rate tunable ultrasonic force regulated nanomachining lithography with an atomic force microscope. Nanotechnology 2012;23(8).
[4] Fang TH, Chang WJ. Effects of AFM-based nanomachining process on aluminum surface. J Phys Chem Solids 2003.
[5] Khurshudov AG, Kato K, Koide H. Nano-wear of the diamond AFM probing tip under scratching of silicon, studied by AFM. Tribol Lett 1996.
[6] Martin-Olmos C et al. Conductivity of SU-8 thin films through atomic force microscopy nano-patterning. Adv Funct Mater 2012.
[7] Deng J, Dong J, Cohen PH. Development and characterization of ultrasonic vibration assisted nanomachining process for three-dimensional nanofabrication. IEEE Trans Nanotechnol 2018;17(3):559–66.
[8] Gozen BA, Ozdoganlar OB. A rotating-tip-based mechanical nanomanufacturing process: nanomilling. Nanoscale Res Lett 2010.
[9] Deng J, Dong J, Cohen P. Rapid fabrication and characterization of SERS substrates. Procedia Manuf 2018;26:580–6.
[10] Wang J, Yan Y, Geng Y, Gan Y, Fang Z. Fabrication of polydimethylsiloxane nanofluidic chips under AFM tip-based nanomilling process. Nanoscale Res Lett 2019;14(1):136.
[11] Zhang J, Cui T, Ge C, Sui Y, Yang H. Review of micro/nano machining by utilizing elliptical vibration cutting. Int J Mach Tools Manuf 2016;106:109–26.
[12] Yan Y, Chang S, Wang T, Geng Y. Scratch on polymer materials using AFM tip-based approach: a review. Polymers Sep. 2019;11:1590.
[13] Shi J, Liu L, Zhou P, Wang F, Wang Y. Subnanomachining by ultrasonic-vibration-assisted atomic force microscopy. IEEE Trans Nanotechnol 2015;14(4):735–41.
[14] Deng J, Zhang L, Dong J, Cohen PH. AFM-based 3D nanofabrication using ultrasonic vibration assisted nanomachining. Procedia Manuf 2015;1:584–92.
[15] Zhang L, Dong J, Cohen PH. Material-insensitive feature depth control and machining force reduction by ultrasonic vibration in AFM-based nanomachining. IEEE Trans Nanotechnol 2013;12(5):743–50.
[16] Mamin HJ. Thermal writing using a heated atomic force microscope tip. Appl Phys Lett 1996;69(3):433–5.
[17] Vettiger P et al. The 'Millipede'—more than thousand tips for future AFM storage. IBM J Res Dev 2000;44(3):323–40.
[18] Lee WK, Sheehan PE. Scanning probe lithography of polymers: tailoring morphology and functionality at the nanometer scale. Scanning 2008;30(2):172–83.
[19] Goode KR, Bowen J, Akhtar N, Robbins PT, Fryer PJ. The effect of temperature on adhesion forces between surfaces and model foods containing whey protein and sugar. J Food Eng 2013;118(4):371–9.
[20] Qu W, Chen X, Ke C. Temperature-dependent frictional properties of ultra-thin boron nitride nanosheets. Appl Phys Lett 2017;110(14):143110.
[21] Fang TH, Da Wu C, Kang SH. Thermomechanical properties of polymer nanolithography using atomic force microscopy. Micron 2011;42(5):492–7.
[22] Pires D et al. Direct write 3-dimensional nanopatterning using probes. Alternative Lithographic Technol II 2010;7637:76371E.
[23] Knoll AW et al. Probe-based 3-D nanolithography using self-amplified depolymerization polymers. Adv Mater 2010;22(31):3361–5.
[24] Holzner F et al. Thermal probe nanolithography: in-situ inspection, high-speed, high-resolution, 3D. 29th European Mask and Lithography Conference 2013;8886:888605.
[25] Broekmaat J, Brinkman A, Blank DHA, Rijnders G. High temperature surface imaging using atomic force microscopy. Appl Phys Lett 2008;92(4):043102.
[26] Eaton PJ, Graham P, Smith JR, Smart JD, Nevell TG, Tsibouklis J. Mapping the surface heterogeneity of a polymer blend: an adhesion-force-distribution study using the atomic force microscope. Langmuir 2000;16(21):7887–90.